NANO · MICRO small
www.small-journal.com

# An Intelligent Graphene-Based Biosensing Device for Cytokine Storm Syndrome Biomarkers Detection in Human Biofluids

*Zhuang Hao, Yang Luo, Cong Huang, Ziran Wang, Guoli Song, Yunlu Pan,* Xuezeng Zhao, and Shaoqin Liu*

**Abnormal elevated levels of cytokines such as interferon (IFN), interleukin (IL), and tumor necrosis factor (TNF), are considered as one of the prognosis biomarkers for indicating the progression to severe or critical COVID-19. Hence, it is of great significance to develop devices for monitoring their levels in COVID-19 patients, and thus enabling detecting COVID-19 patients that are worsening and to treat them before they become critically ill. Here, an intelligent aptameric dual channel graphene-TWEEN 80 field effect transistor (DGTFET) biosensing device for on-site detection of IFN-γ, TNF-α, and IL-6 within 7 min with limits of detection (LODs) of $476 \times 10^{-15}$, $608 \times 10^{-15}$, or $611 \times 10^{-15}$ M respectively in biofluids is presented. Using the customized Android App together with this intelligent device, asymptomatic or mild COVID-19 patients can have a preliminary self-detection of cytokines and get a warning reminder while the condition starts to deteriorate. Also, the device can be fabricated on flexible substrates toward wearable applications for moderate or even critical COVID-19 cases for consistently monitoring cytokines under different deformations. Hence, the intelligent aptameric DGTFET biosensing device is promising to be used for point-of-care applications for monitoring conditions of COVID-19 patients who are in different situations.**

## 1. Introduction

Coronavirus disease 2019 (COVID-19), spreading rapidly throughout the world in early 2020, is a highly pathogenic infectious respiratory system disease and can be easily transmitted from human to human through direct contact. COVID-19 virus infects human epithelial lung cells via specific interactions with the angiotensin converting enzyme 2 (ACE2) (**Figure 1**a).[1,2] At the early of infection, most COVID-19 patients remain asymptomatic or have mild-to-moderate symptoms such as fever, cough, fatigue and myalgia, while a subgroup of patients would become severely ill and have a cytokine storm syndrome (CSS).[3] CSS is a kind of uncontrolled immune activation with excessive release of cytokines including interferon (IFN), interleukin (IL), and tumor necrosis factor (TNF), and could result in acute respiratory distress syndrome (ARDS), multiorgan failure, and even death.[4] Currently, CSS is identified as a poor prognosis for critical COVID-19 cases and abnormal elevations in cytokines levels could be used for indicating the progression to severe or critical COVID-19.[5–7] This consensus is already verified by the clinical data obtained from 41 COVID-19 patients in Jin Yin-tan Hospital, Wuhan, China, at the early beginning of 2020.[8] Hence, it is of great significance to develop devices for monitoring cytokines levels in COVID-19 patients, thereby enabling detecting COVID-19 patients that are worsening and to treat them before they become critically ill. This would be much helpful to avoid oversaturation of the ICU and economize medical sources.

Due to the simple configuration, easy and economic fabrication process, high sensitivity and short response time, aptameric graphene-based field effect transistor (GFET) sensors have been reported for label-free and highly specific recognition of virus, ions, hormones, cells, DNA, glucose, and cytokines.[9–14] However, unwanted interferences generated from changes in environmental condition parameters (e.g., pH and ionic strength) and nonspecific adsorption of complex components in human biofluids always impact the GFET sensing performance and hamper its practical clinical applications.[15–17]

In this work, we present an intelligent aptameric dual channel graphene-TWEEN 80 field effect transistor (DGTFET)

Dr. Z. Hao, C. Huang, Z. Wang, Prof. Y. Pan, Prof. X. Zhao
State Key Laboratory of Robotics and Systems
School of Mechatronics Engineering
Harbin Institute of Technology
Harbin 150001, China
E-mail: yunlupan@hit.edu.cn
Dr. Z. Hao, Prof. S. Liu
School of Chemistry and Chemical Engineering
Harbin Institute of Technology
Harbin 150001, China
Dr. Z. Hao, C. Huang, Z. Wang, Prof. Y. Pan, Prof. X. Zhao, Prof. S. Liu
Key Laboratory of Micro-systems and Micro-structures Manufacturing
Ministry of Education
Harbin Institute of Technology
Harbin 150080, China
Dr. Y. Luo, Prof. G. Song
State Key Laboratory of Robotics
Shenyang Institute of Automation
Chinese Academy of Sciences
Shenyang 110169, China
Prof. S. Liu
State Key Laboratory of Urban Water Resource and Environment
Harbin Institute of Technology
Harbin 150080, China
The ORCID identification number(s) for the author(s) of this article can be found under https://doi.org/10.1002/smll.202101508.

**DOI: 10.1002/smll.202101508**

 

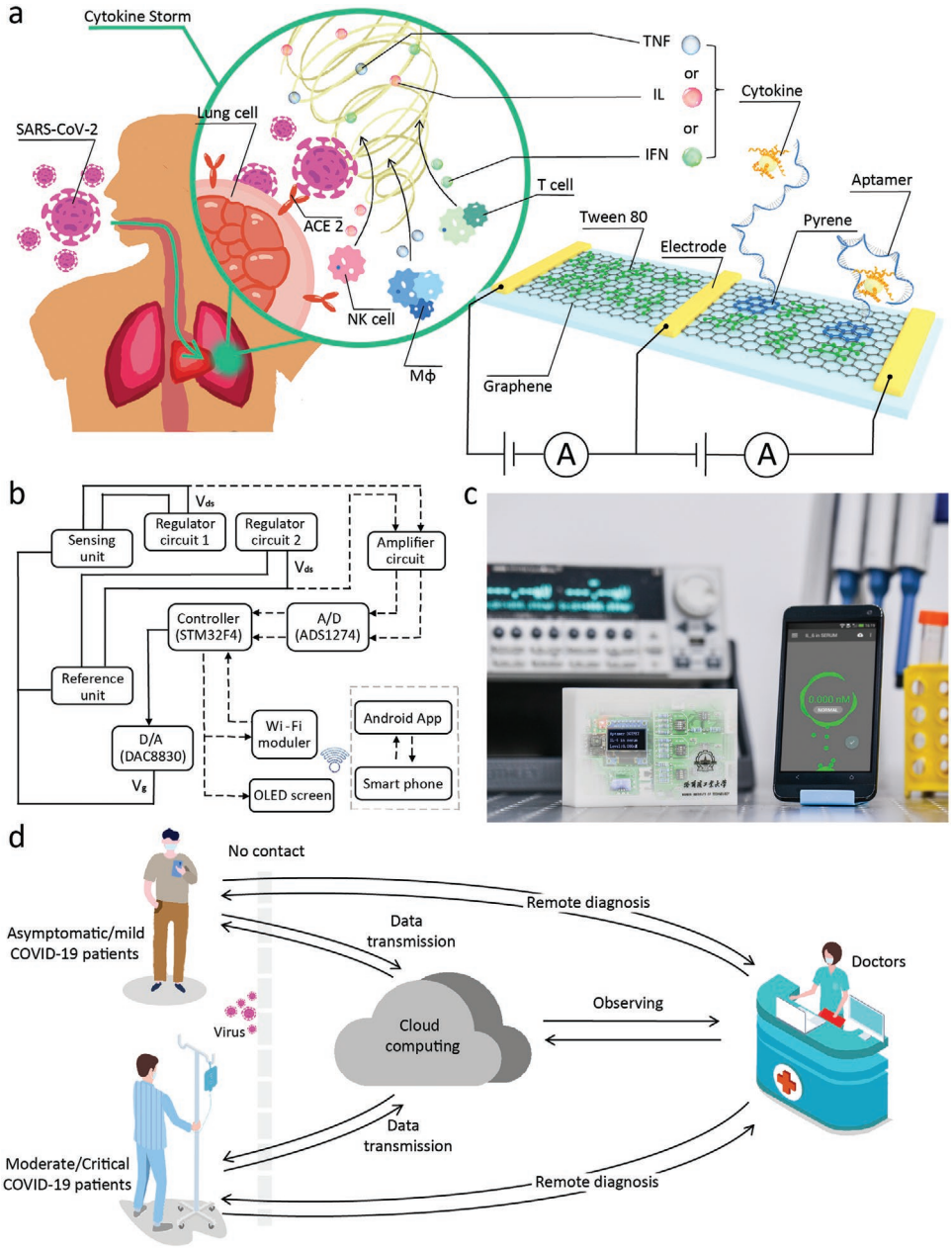


**Figure 1.** The intelligent aptameric DGTFET wireless biosensing device. a) Schematics of the aptameric DGTFET biosensor for detecting biomarkers of cytokine storm syndrome that caused by COVID-19. b) System-level block diagram of the biosensing device showing the power source supply, signal transduction, data processing, information display, and wireless data transmission paths to the mobile phone. c) Photo of the intelligent aptameric DGTFET biosensing device with parts of perspective demonstration and a wireless connected Android smart phone. d) Schematic illustration showing that users can use our device along with a mobile phone for conditions monitoring for COVID-19 patients by detecting abnormal elevation in cytokine levels. Data are transmitted to the user's smart phone and uploaded to cloud for observing by doctors, thus facilitating noncontact remote diagnosis.

biosensing device for on-site and wireless detection of cytokines including IFN, IL, and TNF, in human biofluids such as serum, saliva, urine and sweat, toward applications of health conditions monitoring for COVID-19 patients (Figure 1a–c). In this device, an aptameric DGTFET biosensor chip is integrated in a self-designed wireless electrical measurement device. The aptameric DGTFET biosensor, which can be mass-fabricated, consists of a sensing channel and a reference channel. The sensing channel, graphene in which is functionalized with the target cytokine aptamer, responds to not only the target cytokine but also changes in environmental condition parameters. While the reference channel, graphene in which is without aptamer functionalization, only responds to changes in environmental condition parameters. Due to the low binding affinity to complex components in human biofluids, TWEEN 80 is functionalized on both two graphene channels to form a passivation layer.[18] Final sensor response signal is calculated on the basis of the differential

value between the signal values acquired respectively from the sensing channel and the reference channel. Thanks to the differential measurement design and TWEEN 80 passivation layer, false response signals originated from unwanted background interferences in biofluids can be effectively minimized or eliminated.[19] The entire size of this highly integrated biosensing device is smaller than a mobile phone. A built-in OLED screen is equipped inside for the accurate detection information display. With the aid of an integrated Wi-Fi module and self-designed data processing circuits, which are fabricated on low-cost printed circuit boards (PCBs), the sensor signal transduction and acquisition, on-site differential signal processing, information display and wireless data transmission to an Android mobile-phone and cloud sever can be realized. Moreover, using the customized Android App together with this intelligent device, asymptomatic or mild COVID-19 patients could have a preliminary self-detection of cytokines and get a warning reminder while the condition starts to deteriorate. Simultaneously, results would also be transferred to doctors, thus facilitating noncontact remote diagnosis and reducing the doctor-patient face-to-face contact frequency to lower their risk of infection (Figure 1d).

The aptameric DGTFET's sensing capability is examined in different biofluids using IFN-$\gamma$, IL-6, and TNF-$\alpha$ as representatives. According to experimental results, the sensor can effectively mitigate the influence from unwanted interferences including pH, ionic strength variations and nonspecific adsorption of complex components in biofluids such as serum, saliva, urine, and sweat. Meanwhile, with functionalization of the corresponding aptamer on the sensing channel, the sensor can respond to the IFN-$\gamma$, IL-6, or TNF-$\alpha$ concentration change within 7 min with the limits of detection (LODs) of $476 \times 10^{-15}$, $608 \times 10^{-15}$, or $611 \times 10^{-15}$ M, respectively. Further, we also validate the well sensing performance of the sensor fabricated on ultrathin flexible polyethylene terephthalate (PET) film for monitoring cytokines in sweat toward wearable applications for moderate or even critical COVID-19 cases.

Thus, our intelligent aptameric DGTFET biosensing device is promising to be used for point-of-care applications for monitoring conditions of COVID-19 patients who are in different situations.

## 2. Results and Discussion

### 2.1. Aptameric DGTFET Biosensor Sensing Principle

Detailed description for the working principle of our aptameric DGTFET biosensing device is illustrated in **Figure 2**a,b. In the absence of target cytokines, signals from both sensing and reference channels are slightly and inevitably affected by background interferences, which could be minimized or even eliminated by the differential measurement approach.[19] While being captured by aptamers on the graphene sensing channel, charged cytokine molecules are brought into the electrical double layer (EDL) on the graphene-solution interface, thereby significantly altering the charge distribution on the graphene-solution interface as well as the carrier concentration in the bulk of graphene and generating a significant and detectable change $\Delta I_{ds}$ in drain-source current $I_{ds}$.[11,20] However, without the aid of aptamers, cytokine molecules in the reference channel are not amenable to reach the close vicinity of graphene and excite a significant change in the carrier concentration in graphene.[21] Noted that the binding interaction induced change in the response signal, $\Delta I_{ds}$, is weak. Commercial data collectors are not amenable to acquire accurate original $\Delta I_{ds}$ value for the subsequent analysis due to the influence of instrument noises. Hence, we convert the original current signals $I_{ds,\,sen}$ and $I_{ds,\,ref}$ into voltage signals $V_{amp,\,sen}$ and $V_{amp,\,ref}$ respectively, where $V_{amp,\,sen} = I_{ds,\,sen} \times R_{amp,\,sen}$, $V_{amp,ref} = I_{ds,\,ref} \times R_{amp,\,ref}$ while $R_{amp,\,sen}$ and $R_{amp,\,ref}$ are the zoom resistance of sensing channel and reference channel, respectively. According to the abovementioned aptameric DGTFET biosensor working principle, the mathematical relationship between the response signal and the target cytokine concentration is established and given as

$$\Delta V_{dif} / \Delta V_{dif,max} = A \frac{c^m}{K_D + c^m} \quad (1)$$

where $V_{dif}$ is defined as the differential value of the sensing channel signal $V_{amp,\,sen}$ and the reference channel signal $V_{amp,\,ref}$. Here, to further eliminate nonuniformities originated from sensor fabrication and materials properties, the final response is normalized as the ratio of $\Delta V_{dif}$ and $\Delta V_{dif,\,max}$. $\Delta V_{dif} = V_{dif} - V_{dif,\,0}$, where $V_{dif,0}$ is the value of $V_{dif}$ obtained in buffer at the very beginning. The maximum value of $\Delta V_{dif}$ is defined as $\Delta V_{dif,\,max}$. $A$, $K_D$, and $m$ are saturated coefficient, binding equilibrium constant and Hill coefficient, respectively. Details about the equation establishment can be found in supporting information.

### 2.2. Validity of the Differential Measurement Design and TWEEN 80 Passivation

First, control experiments are conducted to verify the effectiveness of our differential design on the elimination of effects from variations in pH and ionic strength. Here, graphene channels in both sensing and reference channels are untreated. As shown in Figure 2c, with pH increasing from 6.3 to 8.5, the original signals from sensing and reference channels increase stepwise from 0.878 to 0.946 V and 0.577 to 0.623 V, respectively. However, the differential measured value is almost constant around 0, indicating the differential response signal is insensitive to the variations in pH. Additionally, effects from variations in ionic strength are also checked. As shown in Figure 2d, with ionic strength of phosphate buffered solution (PBS) buffer decreasing from 0.5X to 0.01X ($Na^+$: from $67.5 \times 10^{-3}$ to $1.35 \times 10^{-3}$ M), the original signals from sensing and reference channels increase stepwise from 0.269 to 0.312 V and 0.203 to 0.237 V, respectively. While the differential measured value is still invariable at 0, suggesting effects from variations in ionic strength is minimized or even eliminated. Additionally, the validity of our sensor on minimizing or even eliminating nonspecific adsorption of complex components in biofluids is studied (Figure 2e). Here, widely reported single channel aptameric GFET without TWEEN 80 functionalization (hereinafter

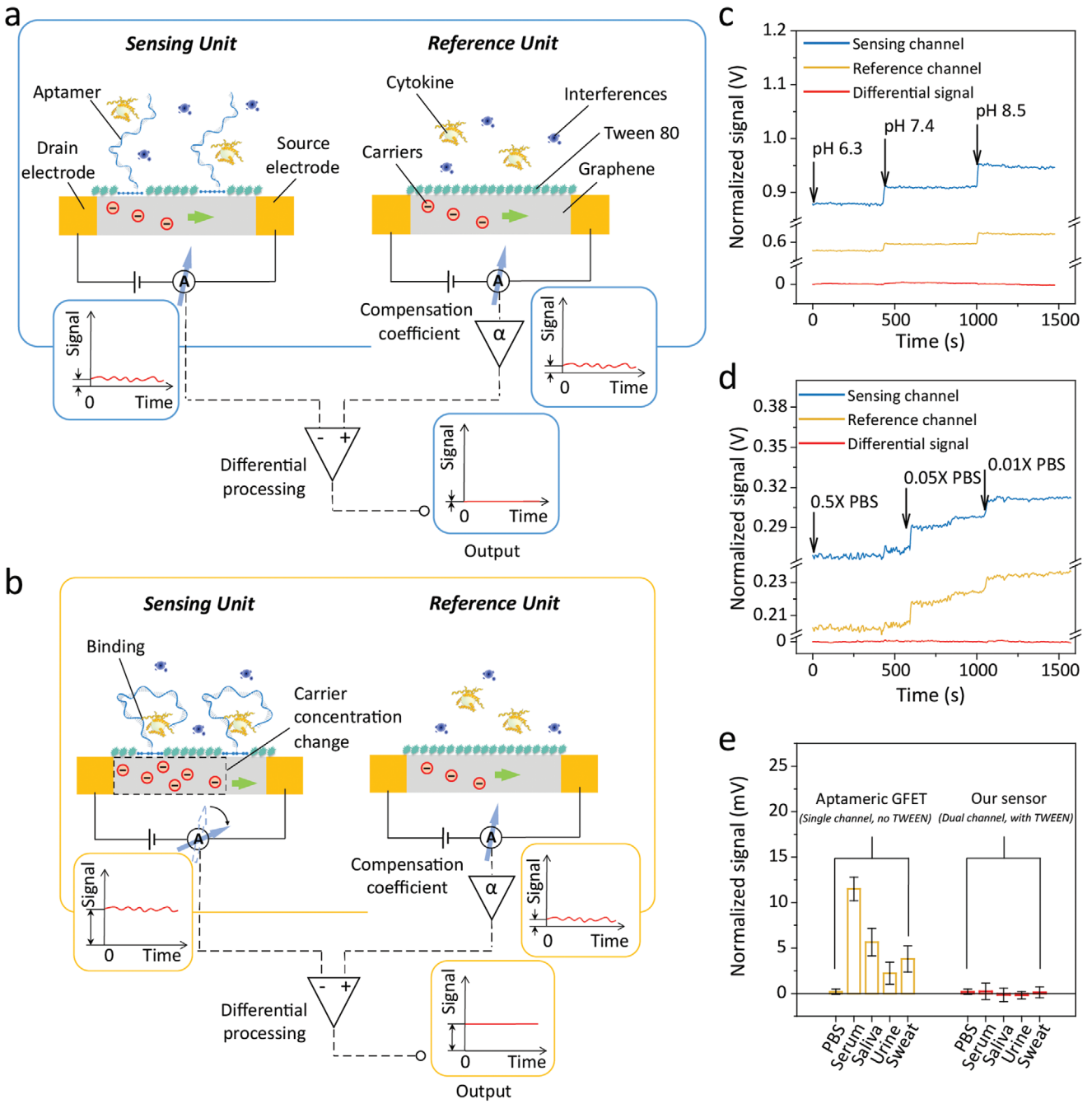


**Figure 2.** Working principle of the aptameric DGTFET biosensor and effects elimination upon the appearance of interferences by the aptameric DGTFET. a,b) Schematics of the working principle of the aptameric DGTFET. c) As-measured signals from sensing channel, reference channel and differential calculation over time in the presence of variations in pH from 6.3 to 8.5. d) As-measured signals from sensing channel, reference channel and differential calculation over time upon the appearance of changes in ionic strength from 0.5X to 0.01X ($Na^+$: from 67.5 to 1.35 × $10^{-3}$ M). e) Normalized signals for reported aptameric GFET and our sensor upon incubation of undiluted solutions including 1X PBS, serum, saliva, urine, and sweat, respectively.

referred to as aptameric GFET) is employed as a comparison object. Different types of undiluted solutions including 1X PBS, serum, saliva, urine, and sweat are sequentially incubated onto graphene channels of GFET and our sensor. It can be seen normalized aptameric GFET response signal is significantly varied after graphene exposure to undiluted biofluids including serum, saliva, urine, and sweat. However, thanks to the TWEEN 80 passivation and differential measurement approach, our sensor response is almost kept constant around 0 under different conditions. Hence, it can be concluded background interferences from biofluids can be effectively minimized or eliminated by our sensor.

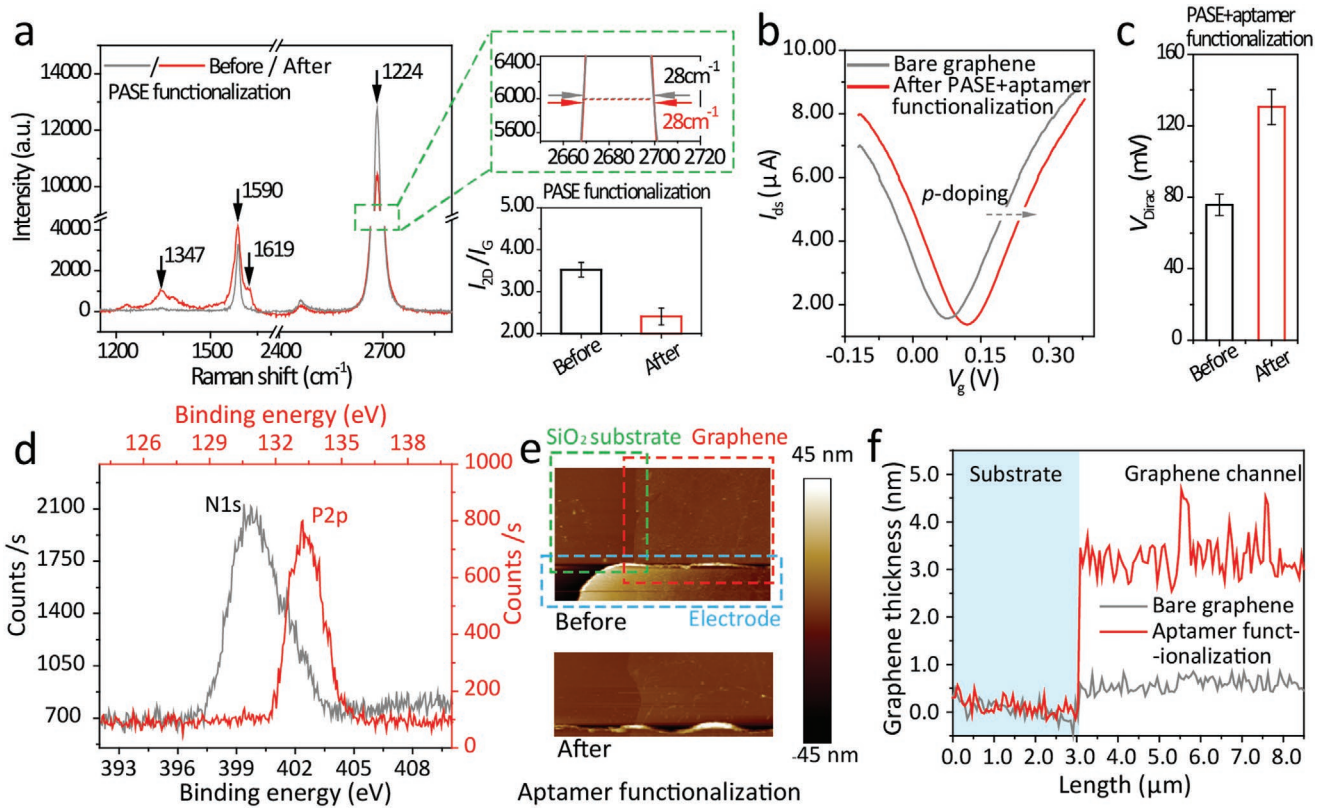


**Figure 3.** Graphene characterization after biochemical functionalization. a) Distinct peaks and peak intensity changes of the graphene–pyrene interaction are seen after immersing in PASE in the Raman spectra of graphene. b,c) Graphene transfer curve has a significant positive shift with $V_{Dirac}$ decreased from 78 to 130 mV after PASE and aptamer immobilization. d) XPS showing the peak of the phosphorus element and nitrogen element on graphene after immersing in PASE. e) Surface topographies of the graphene surface before and after IFN-$\gamma$ aptamer functionalization are characterized by AFM. Scale bar: 5 μm. The thickness of graphene sensing channel is seen to be increased from 0.4 to 3.2 nm after the IFN-$\gamma$ aptamer functionalization f).

### 2.3. Characterization of the Graphene Surface Biochemical Functionalization

To realize the target cytokine detection, its aptamer, a single strand oligonucleotides consisting of a given numbers and types of nucleobases that ordered in a specific sequence, should be immobilized on graphene via the Schiff-base reaction with linkers such as 1-pyrenebutanoic acid succinimidyl ester (PASE) first. To examine the success of PASE and aptamer functionalization, the graphene surface is characterized after each functionalization step, respectively. The functionalization methods for IFN-$\gamma$, IL-6, and TNF-$\alpha$ aptamers are exactly the same. Also, the characterization methods to verify their successful functionalization are also exactly the same. Here, IFN-$\gamma$ aptamer is chosen as a representative. In **Figure 3**a, the Raman spectra of the PASE functionalized graphene exhibits a distinct peak at 1347 $cm^{-1}$ and a G-peak splitting at 1619 $cm^{-1}$ owing to the $\pi$–$\pi$ stacking interaction between graphene and the pyrene group in PASE. The full width at half maximum (FWHM) of the 2D band is always 28 $cm^{-1}$ from Lorentz fitting before and after PASE functionalization can be used as the evidence of monolayer graphene, which could provide a higher sensitivity than multilayers graphene.[22] The ratio of the intensity of 2D band to G band ($I_{2D}/I_G$) decreases from 3.65 to 2.32 is considered as a result of chemical doping from PASE.[23] In conclusion, the immobilization of PASE is successful. On the other hand, after PASE and aptamer functionalization, a significant positive shift of the graphene transfer curve with $V_{Dirac}$, where $I_{ds}$ reaches its minimum, increases from 78 to 130 mV (Figure 3b,c).[24] X-ray photoelectron spectroscopy (XPS) indicates PASE constituent element nitrogen and aptamer constituent element phosphorus can be easily found at 399.74 eV and 133.33 eV after PASE and aptamer functionalization, respectively (Figure 3d). Further, as AFM images shown, the thickness of the graphene sensing channel also increases from 0.4 to 3.2 nm (Figure 3e,f).[11,25,26] These experimental results suggest that PASE and aptamer have been functionalized on graphene successfully.[27,28]

### 2.4. Investigation of the Senor Sensing Capability for Cytokines Detection

Subsequntly, detection of IFN-$\gamma$, IL-6, and TNF-$\alpha$ in PBS buffer are performed, respectively. After IFN-$\gamma$ specific aptamer functionalization on the sensing channel graphene, real-time detection of IFN-$\gamma$ is carried out on the device with a constant $V_{ds}$ at 12 mV and $V_g$ at 75 mV. After each IFN-$\gamma$ solution addition and the aptamer-IFN-$\gamma$ binding reached equilibrium (around 7 min), time-resolved sensor response signal was measured and plotted in **Figure 4**a. With ascending IFN-$\gamma$ concentrations from buffer

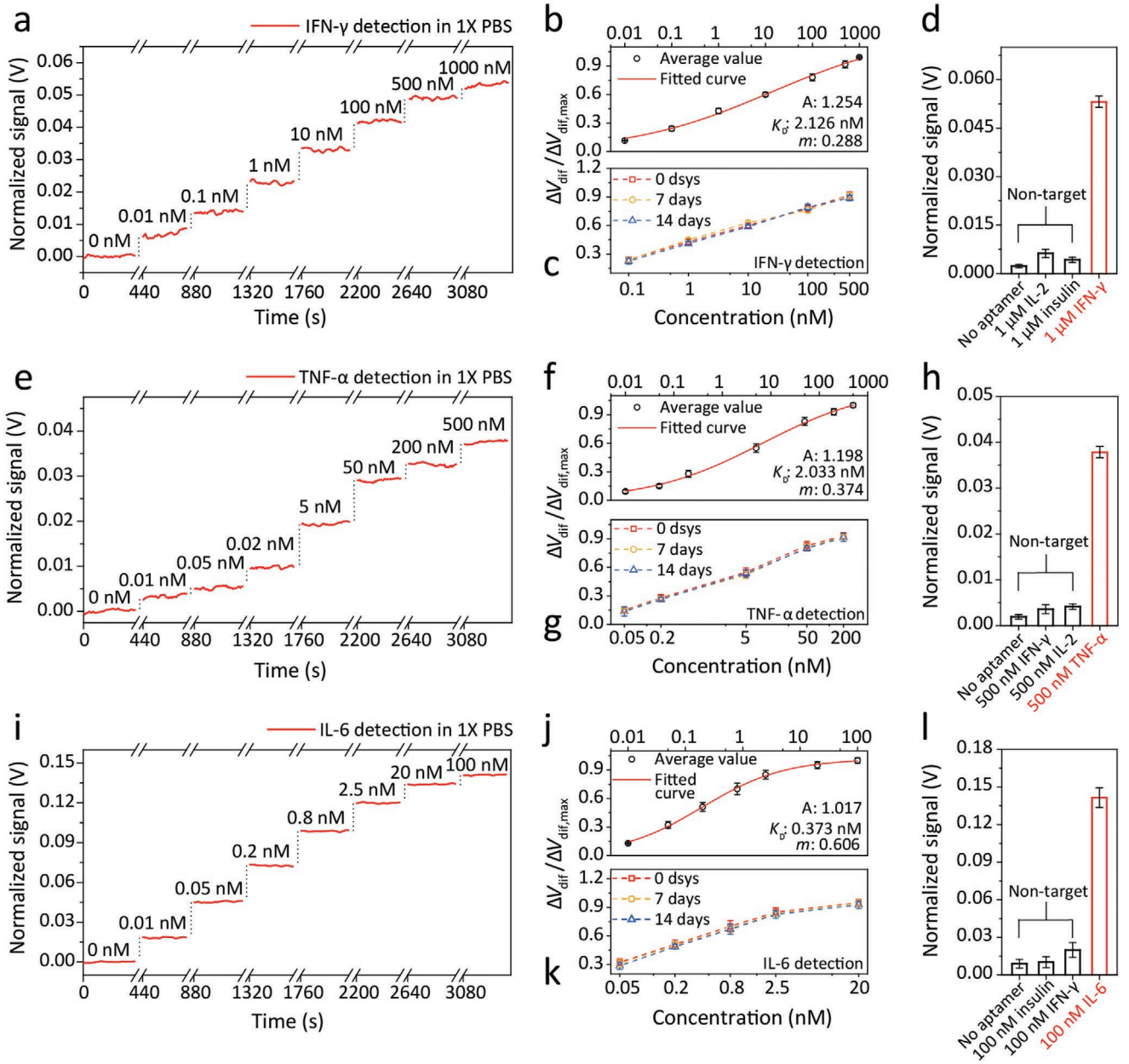


**Figure 4.** Cytokines detection in 1X PBS. a) Time-resolved sensor signal to different concentration IFN-$\gamma$ solutions. b) Changes in the mean value of normalized signals measured at equilibrium as a function of IFN-$\gamma$ concentrations. The red line is a least-squares fit to Equation (1). c) Characterization of the aptameric DGTFET biosensor consistency for IFN-$\gamma$ detection after storage in 1X PBS at 4 °C for 7 and 14 days, respectively. d) Normalized selective response obtained at the same concentration for target IFN-$\gamma$ and other nontarget molecules including error bars. The similar experiments are carried out for TNF-$\alpha$ and IL-6 with results shown in (e–h) and (i–l), respectively.

to $1 \times 10^{-6}$ M, the differential signal $V_{dif}$ increases from 0 to 0.054 V stepwise and monotonically. The final response signal $\Delta V_{dif}/\Delta V_{dif,\,max}$ at different IFN-$\gamma$ concentrations is plotted as a function of the IFN-$\gamma$ concentration in Figure 4b with error bars obtained from three different devices.

We also find the data points could be well described by our established cytokine concentration and DGTFET response mathematical model (Equation (1)). On the basis of the fitted curve demonstrated in Figure 4b, saturated coefficient $A$, binding equilibrium constant $K_D$ and Hill coefficient $m$ are estimated to be 1.254, $2.125 \times 10^{-9}$ M, and 0.288, respectively. According to the $3\sigma$ rule,[29] the limit of detection (LOD) for IFN-$\gamma$ detection of the DGTFET biosensing device is calculated to be $476 \times 10^{-15}$ M, which is much lower than the LODs that obtained by previously reported IFN-$\gamma$ sensors,[9,30] indicating the high sensitivity of our sensor. Then, the effect from extended-time storage on the consistency and reliability of our sensor is investigated. After the aptamer functionalization, detection of IFN-$\gamma$ with various concentrations ($0.1 \times 10^{-9}$, $1 \times 10^{-9}$, $10 \times 10^{-9}$, $100 \times 10^{-9}$, and $500 \times 10^{-9}$ M) is performed

after storing the aptameric DGTFET sensor chip in 1X PBS at 4 °C for 7 and 14 days, respectively. Normalized signals with error bars obtained from no less than three devices are plotted in Figure 4c along with the data extracted from Figure 4b. Almost consistent detection results at each concentration with a deviation less than 7% indicates the good reliability of our sensor.[31] To evaluate the selectivity of our sensor to IFN-$\gamma$, control experiments are conducted with no aptamer functionalized graphene exposure to IFN-$\gamma$ and the aptamer functionalized graphene exposure to nontarget molecules insulin and IL-2 at $1 \times 10^{-6}$ M. As shown in Figure 4d, the signal value for $1 \times 10^{-6}$ M IFN-$\gamma$ is 0.053 V, which is over 8.5 times bigger compared with the values obtained under other conditions, indicating the high sensor selectivity to IFN-$\gamma$.[12,32]

On the other hand, detection of IL-6 and TNF-$\alpha$ in PBS are also conducted respectively with their specific aptamers functionalized on the sensing channels under the same conditions using different devices. For IL-6, as shown in Figure 4e,f, coefficient A, $K_D$, $m$, and LOD are estimated to be 1.017, $0.373 \times 10^{-9}$ M, 0.606, and $608 \times 10^{-15}$ M, respectively. Experimental results demonstrated in Figure 4g,h suggest promising reliability and selectivity for our sensor in IL-6 detection are obtained. Also, similar results can be found in the TNF-$\alpha$ detection with an estimated LOD of $611 \times 10^{-15}$ (Figure 4i–l). Thus, our sensor holding competitive LODs paves a new way for highly sensitive and rapid cytokines detection.[33]

### 2.5. Cytokines Detection in Biofluids

To evaluate our sensor for cytokines detection in real world biofluids, detection of IFN-$\gamma$, IL-6, and TNF-$\alpha$ in various biofluids are carried out with the aid of the APP, respectively. The APP interface for each step and instructions are demonstrated in **Figure 5**a. Before tests, the user should select biofluids types and detection targets. If the detected cytokine level is within a normal range, a green "normal" sign circled around the detected level value would appear. However, an "abnormal" sign would replace of the "normal" sign with green turning into red while the detected cytokine level is out of the normal range. Also, if the cytokine level values, which are detected during the past several days and already recorded in history, keep climbing, the App would also give an alert to remind the user even they are presently within the normal range.

Here, serum, saliva and urine are all used to examine our sensor's sensing capability. Human saliva and human urine are collected as described in experimental section. Commercial fetal calf serum is used in place of human serum. First, IFN-$\gamma$ specific aptamer is functionalized on the sensing channel graphene. Then, IFN-$\gamma$ lyophilized powder is dissolved with serum, saliva, and urine to given concentrations ($5 \times 10^{-12}$, $10 \times 10^{-12}$, $20 \times 10^{-12}$, and $50 \times 10^{-12}$ M) for tests, respectively. After adding 40 µL IFN-$\gamma$ solution of a given concentration onto the graphene surface and waiting for 7 min, the IFN-$\gamma$ level is measured using the mobile phone App (Figure 5b). For each given concentration, the same experiment is repeated using five different devices. The average value with error bars for the five measured levels $C_{me}$ is plotted in Figure 5c–e (columns). Also, the sensor accuracy is defined as the ratio of the real level $C_{re}$ and the absolute differential value of $C_{re}$ and $|C_{re} - C_{me}|$, which is the absolute differential value of $C_{me}$ and $C_{re}$, and shown in Figure 5c–e (dots). Obviously, the lowest sensor accuracy value obtained under different conditions is always lager than 95.48%, indicating the remarkable IFN-$\gamma$ detection capability of our sensor in biofluids including serum, saliva and urine. Additionally, with functionalization of TNF-$\alpha$ aptamer (IL-6 aptamer), same detection experiments of TNF-$\alpha$ (IL-6) are conducted in serum, saliva and urine, respectively. Detection results shown in Figure 5f–h (Figure 5i–k) demonstrate that the sensor accuracy is over 95.2% (95.8%), suggesting our sensor is amenable to detect various kinds of cytokines under complex environmental conditions with the aid of the target cytokine specific aptamer.

### 2.6. Flexible Aptameric DGTFET

Moderate and critical COVID-19 patients often experience persistent symptoms of fever, sweating, weakness and even coma, making it hard for them to do the self-test frequently. Considering these, our aptameric DGTFET biosensor that fabricated on ultrathin flexible PET film could be controlled by doctors remotely through Wi-Fi and is promising to be comfortably worn on different body parts for monitoring patients' body conditions trough real-time detecting sweat cytokines levels (**Figure 6**a).[34–37] We first examine the flexible sensor stability under different deformation conditions. As the folding angles or twisting angles vary from −180° to 180°, the change in a graphene channel transconductance, a recognized measure of the graphene sensitivity, is much small. Compared to the initial hole branch and electron branch transconductance values (−31.5 and 29.6 µS) measured under flat status, the maximum are 4.1% and 3.7%, respectively (Figure 6b–d). Thus, the electrical properties of the graphene channel remain consistent under the large deformations.[32,38,39] Moreover, the sensor, twisted by 180° and folded by 180°, respectively, is tested for capability of IFN-$\gamma$, TNF-$\alpha$, and IL-6 detection. As shown in Figure 6e, the sensor response holds a high level of consistency, with deviations respectively less than 6.68%, 8.44%, and 7.3%, at any given TNF-$\alpha$ concentration under different deformation conditions. It is concluded that the response of our sensor affords a high level of consistency in cytokine measurements during the deformation tests.

Subsequently, preliminary experiments of real-time monitoring cytokines in human sweat are performed. Time-resolved sensor response to addition of IFN-$\gamma$ solutions at concentration of $10 \times 10^{-12}$ M, $100 \times 10^{-12}$ M, and $1 \times 10^{-9}$ M are measured and plotted in Figure 6f left graph, respectively. It can be seen after $10 \times 10^{-12}$ M, $100 \times 10^{-12}$ M, and $1 \times 10^{-9}$ M IFN-$\gamma$ addition the normalized sensor response signal increases sharply over time and levels off gradually until stabilizes at 0.0058, 0.0137, and 0.0227 V in 380, 330, and 290 s, respectively. Similar experiments results are also observed for $10 \times 10^{-12}$ M/$50 \times 10^{-12}$ M/$200 \times 10^{-12}$ M TNF-$\alpha$ (Figure 6f, mid graph) and $10 \times 10^{-12}$ M/$50 \times 10^{-12}$ M/$200 \times 10^{-12}$ M IL-6 (Figure 6f, right graph) detection. Hence, our flexible DGTFET holds great potential for wearable sweat cytokines monitoring applications.

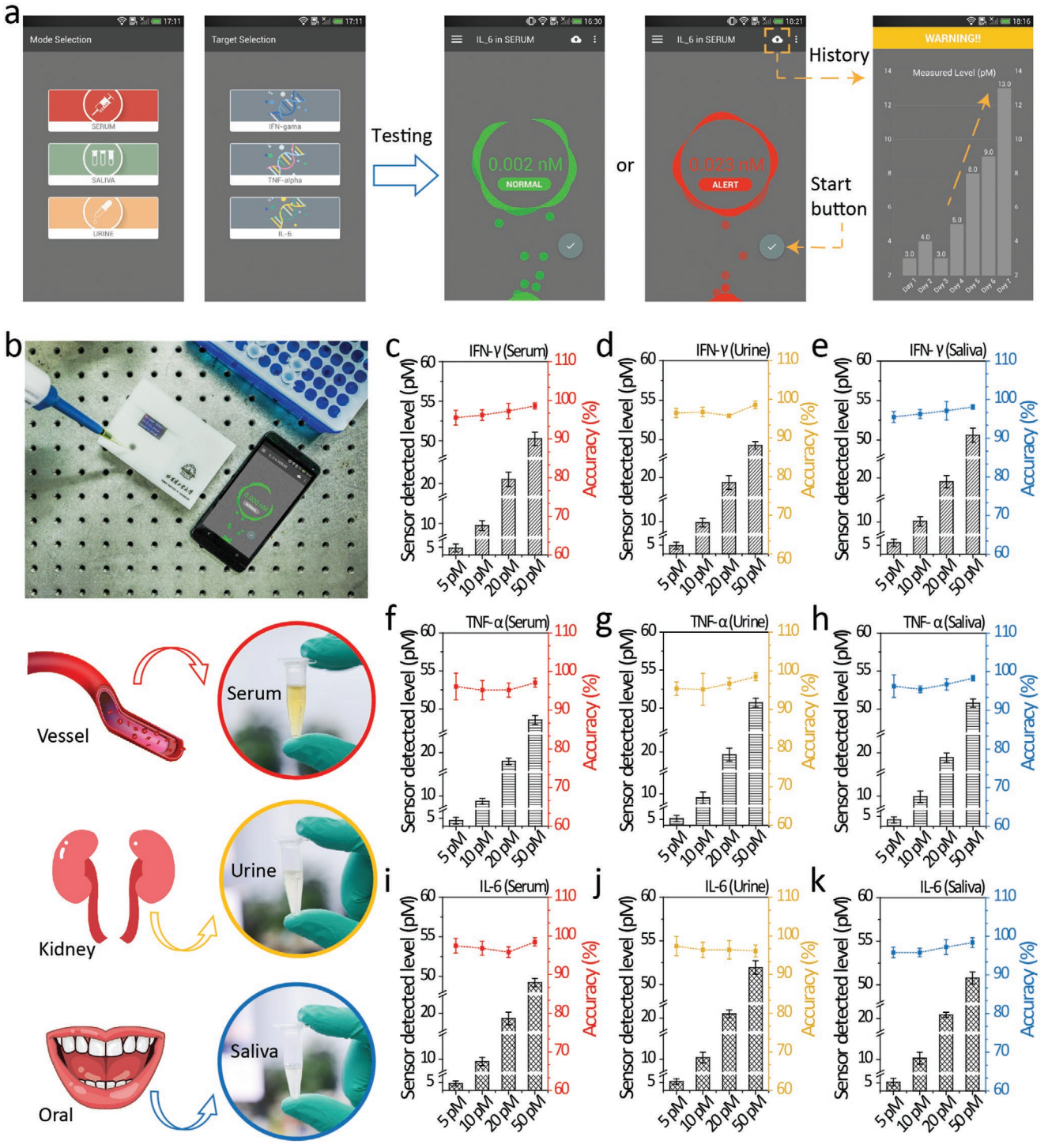


**Figure 5.** Cytokines detection in biofluids. a) The APP interface for each step and instructions. Serum IL-6 detection process is demonstrated as a representative for illustration. b) Photos of the sample solution incubation process using a pipette and collected biofluids samples including serum, urine and saliva. Detection of different concentrations of IFN-$\gamma$ in c) serum, d) urine, and e) saliva, respectively. Detection of different concentrations of TNF-$\alpha$ in f) serum, g) urine, and h) saliva, respectively. Detection of different concentrations of IL-6 in i) serum, j) urine, and k) saliva, respectively.

## 3. Conclusion

To summarize, an intelligent aptameric DGTFET biosensing device is presented for efficient detection of useful CSS prognosis biomarkers IFN-$\gamma$, TNF-$\alpha$, and IL-6 cytokines. Due to the employment of the differential measurement approach and TWEEN 80 passivation, effects from background interferences such as ionic strength changes, pH changes and non-specific adsorption from complex biofluids can be effectively minimized or eliminated. Additionally, through the customized

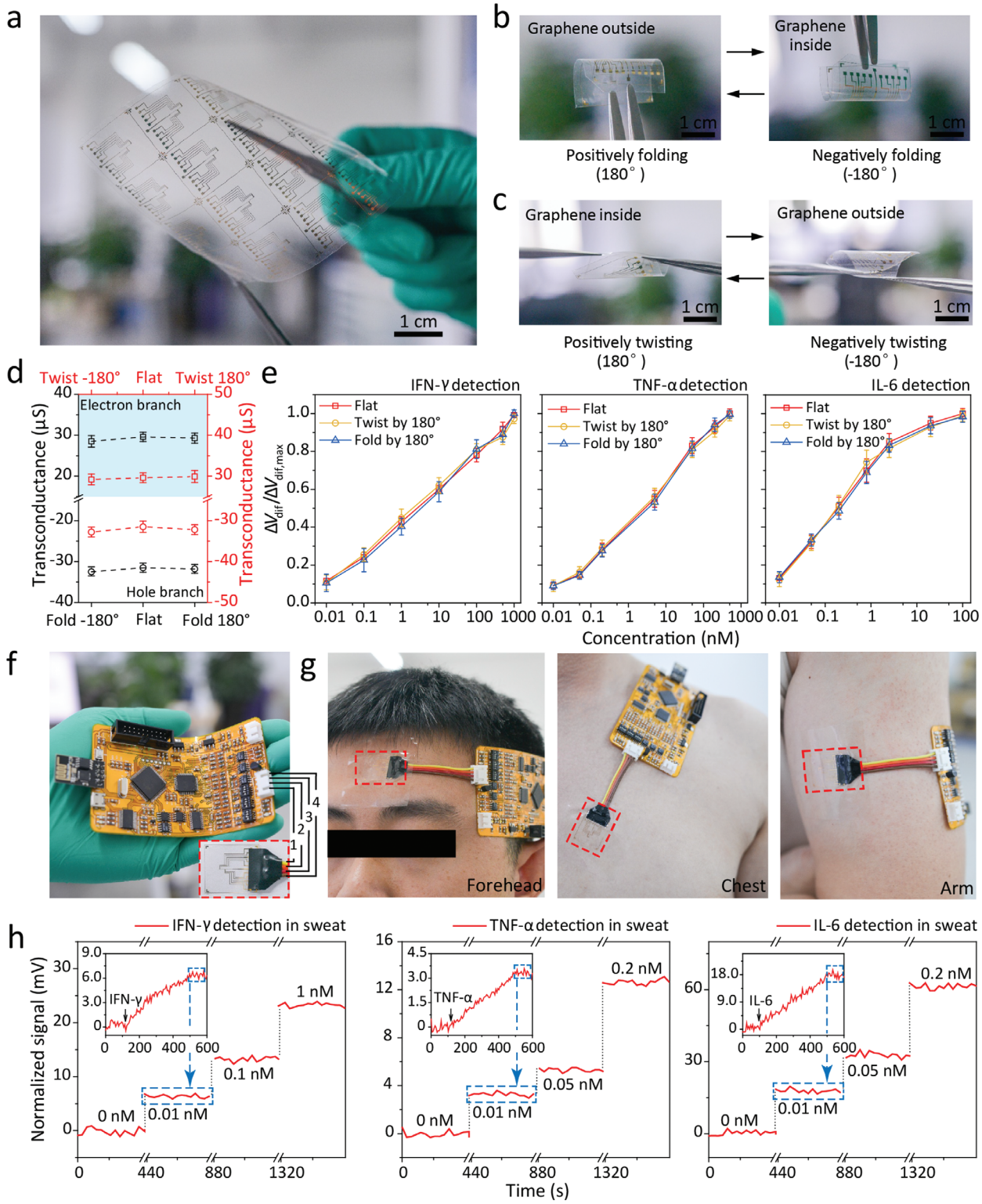


**Figure 6.** Flexible aptameric DGTFET biosensing device and its preliminary wearable application of cytokines detection in sweat. a) Scalable production of the DGTFET arrays on a 25 μm thick flexible PET substrate. b) Illustration of a folding cycle from positive 180° to negative 180° for a single device. c) Illustration of a twisting cycle from positive 180° to negative 180° for a single device. d) Transconductance of the sensor under different deformation conditions. e) Detection of cytokines at different concentrations under different deformation conditions. f) Photograph of a flexible aptameric DGTFET biosensing electrical device. Four wires: 1) Sensing channel signal. 2) Ground. 3) Gate voltage. 4) Reference channel signal. g) The fully integrated device could be comfortably worn on different human body parts such as forehead, chest, and arm. h) Time-resolved measurement of cytokines including IFN-$\gamma$, TNF-$\alpha$, and IL-6 at different concentrations in human sweat.

electrical circuits and Android App, the intelligent device could on-site process the cytokines detection data and provide a preliminary detected cytokine concentration value itself and give a warning reminder while the condiction starts to get worse. We demonstrate this intelligent biosensing device, which also can be transferred on to flexible substrates for wearable applications, is amenable to accurately, rapidly (around 7 min) and reliably detect cytokines IFN-$\gamma$, TNF-$\alpha$, and IL-6 in biofluids including serum, saliva, urine and sweat, with respective LODs of $476 \times 10^{-15}$, $611 \times 10^{-15}$, and $608 \times 10^{-15}$ M, suggesting a promising strategy for applications for monitoring conditions of COVID-19 patients who are in different situations is provided.

## 4. Experimental Section

*Materials*: PASE, PDMS, dimethylformamide (DMF), human insulin, cytokine IL-2, and cytokine IFN-$\gamma$ were ordered from Sigma-Aldrich (St. Louis, MO). 1X PBS at pH = 7.4 was ordered from Thermo Fisher Scientific (Waltham, MA). 285 nm silicon oxide covered silicon wafer was ordered from UniversityWafer (Boston, MA). Copper-base chemical vapor deposition (CVD) graphene was ordered from Graphenea (Cambridge, MA). The sterile synthetic swab used for human saliva sampling was purchased from Salivette (Sarstedt, Germany). Cytokine TNF-$\alpha$ was purchased from R&D Systems (Minneapolis, MN). Cytokine IL-6 was purchased from ACRO Biosystems (Newark, DE). Specific aptamers for IFN-$\gamma$ (sequence 5'-$NH_2$- GGG GTT GGT TGT GTT GGG TGT TGT GT -3'),[14] TNF-$\alpha$ (sequence 5'-$NH_2$- TGG TGG ATG GCG CAG TCG GCG ACA A-3')[9,40] and IL-6 (sequence 5'-$NH_2$- GGT GGC AGG AGG ACT ATT TAT TTG CTT TTC T-3')[41] were synthesized and purified by Sangong Biotech (Shanghai, China). Fetal calf serum was purchased from Tianhang (Zhejiang, China). 25 µm thick polyethylene terephthalate (PET) film was ordered from Dupont Hongji Films (Guangdong, China).

*DGTFET Chip Fabrication*: The 285 nm silicon oxide covered silicon wafer employed as the DGTFET substrate was cleaned successively with acetone, isopropanol (IPA) and ion distilled water, and finally dried by nitrogen and treated by oxygen plasma for few minutes. Metal electrodes of the sensing and reference channels were fabricated via a bilayer lift-off photolithography technique. 2 µm sacrificial layer photoresist LOR 3A and 1.2 µm photoresist S1813 were sequentially spin-coated on the wafer. The planar drain and source electrodes of the two channels and the shared gate electrode consisting of a chromium/gold structure (2 nm/43 nm) were deposited on the wafer using standard photolithography and E-beam metal deposition techniques. Subsequently, the wafer was immersed in Remover PG for 12 hours at room temperature for to remove photoresists.

Additionally, the sensor chip was exposed to oxygen plasma to remove the remaining residue on the substrate surface (Figure S1, Supporting Information). Then, the CVD graphene sheet was transferred onto the wafer to cover the sensing and reference channel areas. To pattern the CVD graphene sheet into two rectangle shapes that stretch over drain-source electrodes of the two channels respectively, 1.2 µm photoresist S1813 layer was spin coated on graphene in turn for photolithography. After exposure with given time and the photoresist developing using developer AZ MIF 300, graphene in the unprotected area was etched by oxygen plasma to create a regular rectangle shape conducting channel (Figure S2, Supporting Information). The sensor chip was fixed onto the PCB board using double-coating tape with electrodes connected to the PCB board embedded bonding pads through silver epoxy glue and fine copper wires. At last, a 3D printed shell was used to encapsulate the entire device (Figure S3, Supporting Information). Details about the circuits design can be found in supporting information (Figure S4, Supporting Information).

*Aptameric DGTFET Biosensor Functionalization*: Graphene surface functionalization for the two channels were realized separately using a polydimethylsiloxane (PDMS) made dual-opening well, which was mounted on the top of the sensor. $5 \times 10^{-3}$ M PASE solution (dissolved in DMF) was incubated into the well of the sensing channel for 2 hours at 25 °C. Then the sensing channel was successively rinsed with pure DMF, ethanol and ion distilled water to remove free PASE. The PASE linker which contains a pyrenyl group, can irreversibly anchor on graphene through $\pi$-$\pi$ stacking. Subsequently, the sensing channel was rinsed using 1X PBS followed by incubation with $5 \times 10^{-6}$ M cytokine aptamer solution for 12 hours at 4 °C. Finally, after rinsing with 1X PBS, $100 \times 10^{-3}$ M ethanolamine solution was added onto the graphene sensing channel for 1 hour to deactivate and block the redundant reactive groups in PASE. Afterward, the sensor chip was immersed in 0.1% Tween 80 solution to passivate all the uncoated graphene area.

*Biofluids Preparation*: 1) Commercial fetal calf serum was used to mimic the real serum environment for cytokine detection experiments. 2) Human saliva sampling was performed using the sterile synthetic swab as sampling device. A 30 years old healthy volunteer (male) is asked to move the swab 2 min in the oral cavity at a self-selected pace. Saliva was then recovered by centrifugation of the swabs at 5000 rpm for 5 min at room temperature (25 °C). Subsequently, the centrifuged suspension was collected and then stored at 2 °C before biomarker solution configurations.[42] 3) Human urine was collected from a 30 years old healthy volunteer (male) in the morning before taking breakfast.[43,44] 4) Human sweat sampling was performed by a 26 years old healthy volunteer (male) using a sweat collection capsule after 30 min exercise. The capsule consists of an adhesive and disposable membrane which could be attached to the forehead, forearm or neck with a fluid-tight window giving access to collect sweat.[9] The collected sweat sample was stored at 2 °C before biomarker solution configurations. The experiments involving human subjects have been performed with the full, informed consent of the volunteers. The institutional ethics board considers sweat, saliva, urine as human waste, not tissue samples, therefore approval was not needed before use.

## Supporting Information

Supporting Information is available from the Wiley Online Library or from the author.

## Acknowledgements

Z.H. and Y.L. contributed equally to this work. This work was supported by the National Natural Science Foundation of China (Grant Nos. 52005137 and 51975145), the China Postdoctoral Science Foundation (Grant No. 2019M661270), the Heilongjiang Postdoctoral Science Foundation (Grant No. LBH-Z19221), and the National Postdoctoral Program for Innovative Talents (Grant No. BX20200105).

## Conflict of Interest

The authors declare no conflict of interest.

## Data Availability Statement

Research data are not shared.

## Keywords

COVID-19, cytokine storm syndrome, graphene, wearable biosensor, wireless and on-site biosensing

Received: March 24, 2021
Revised: April 11, 2021
Published online:

[1] A. J. Wilk, A. Rustagi, N. Q. Zhao, J. Roque, G. J. Martínez-Colón, J. L. McKechnie, G. T. Ivison, T. Ranganath, R. Vergara, T. Hollis, L. J. Simpson, P. Grant, A. Subramanian, A. J. Rogers, C. A. Blish, *Nat. Med.* **2020**, *26*, 1070.
[2] F. Zhang, R. Gan, Z. Zhen, X. Hu, X. Li, F. Zhou, Y. Liu, C. Chen, S. Xie, B. Zhang, X. Wu, Z. Huang, *Signal Transduction Targeted Ther.* **2020**, *5*, 156.
[3] S. F. Pedersen, Y. C. Ho, *J. Clin. Invest.* **2020**, *130*, 2202.
[4] L. A. Henderson, S. W. Canna, G. S. Schulert, S. Volpi, P. Y. Lee, K. F. Kernan, R. Caricchio, S. Mahmud, M. M. Hazen, O. Halyabar, K. J. Hoyt, J. Han, A. A. Grom, M. Gattorno, A. Ravelli, F. De Benedetti, E. M. Behrens, R. Q. Cron, P. A. Nigrovic, *Arthritis Rheumatol.* **2020**, *72*, 1059.
[5] J. B. Moore, C. H. June, *Science* **2020**, *368*, 473.
[6] S. M. Russell, A. Alba-Patiño, E. Barón, M. Borges, M. Gonzalez-Freire, R. De La Rica, *ACS Sens.* **2020**, *5*, 1506.
[7] A. Shakeri, N. A. Jarad, J. Terryberry, S. Khan, A. Leung, S. Chen, T. F. Didar, *Small* **2020**, *16*, 2003844.
[8] C. Huang, Y. Wang, X. Li, L. Ren, J. Zhao, Y. Hu, L. Zhang, G. Fan, J. Xu, X. Gu, Z. Cheng, T. Yu, J. Xia, Y. Wei, W. Wu, X. Xie, W. Yin, H. Li, M. Liu, Y. Xiao, H. Gao, L. Guo, J. Xie, G. Wang, R. Jiang, Z. Gao, Q. Jin, J. Wang, B. Cao, *Lancet* **2020**, *395*, 497.
[9] Z. Wang, Z. Hao, X. Wang, C. Huang, Q. Lin, X. Zhao, Y. Pan, *Adv. Funct. Mater.* **2020**, *31*, 2005958.
[10] Y. Li, C. Wang, Y. Zhu, X. Zhou, Y. Xiang, M. He, S. Zeng, *Biosens. Bioelectron.* **2017**, *89*, 758.
[11] Z. Hao, Y. Zhu, X. Wang, P. G. Rotti, C. Dimarco, S. R. Tyler, X. Zhao, J. F. Engelhardt, J. Hone, Q. Lin, *ACS Appl. Mater. Interfaces* **2017**, *9*, 27504.
[12] B. Cai, S. Wang, L. Huang, Y. Ning, Z. Zhang, G. J. Zhang, *ACS Nano* **2014**, *8*, 2632.
[13] G. Seo, G. Lee, M. J. Kim, S. H. Baek, M. Choi, K. B. Ku, C. S. Lee, S. Jun, D. Park, H. G. Kim, S. J. Kim, J. O. Lee, B. T. Kim, E. C. Park, S. Il Kim, *ACS Nano* **2020**, *14*, 5135.
[14] Z. Wang, Z. Hao, S. Yu, C. G. De Moraes, L. H. Suh, X. Zhao, Q. Lin, *Adv. Funct. Mater.* **2019**, *29*, 1905202.
[15] J. Kim, M. Kim, M. S. Lee, K. Kim, S. Ji, Y. T. Kim, J. Park, K. Na, K. H. Bae, H. K. Kim, F. Bien, C. Y. Lee, J. U. Park, *Nat. Commun.* **2017**, *8*, 14997.
[16] W. Fu, L. Jiang, E. P. van Geest, L. M. C. Lima, G. F. Schneider, *Adv. Mater.* **2017**, *29*, 1603610.
[17] J. Park, J. Kim, S. Y. Kim, W. H. Cheong, J. Jang, Y. G. Park, K. Na, Y. T. Kim, J. H. Heo, C. Y. Lee, J. H. Lee, F. Bien, J. U. Park, *Sci. Adv.* **2018**, *4*, eaap9841.
[18] H. K. Chang, F. N. Ishikawa, R. Zhang, R. Datar, R. J. Cote, M. E. Thompson, C. Zhou, *ACS Nano* **2011**, *5*, 9883.
[19] Y. Li, Y. Zhu, C. Wang, M. He, Q. Lin, *Biosens. Bioelectron.* **2019**, *126*, 59.
[20] B. Zhan, C. Li, J. Yang, G. Jenkins, W. Huang, X. Dong, *Small* **2014**, *10*, 4042.
[21] N. Nakatsuka, K. A. Yang, J. M. Abendroth, K. M. Cheung, X. Xu, H. Yang, C. Zhao, B. Zhu, Y. S. Rim, Y. Yang, P. S. Weiss, M. N. Stojanović, A. M. Andrews, *Science* **2018**, *362*, 319.
[22] Y. Zhu, Y. Hao, E. A. Adogla, J. Yan, D. Li, K. Xu, Q. Wang, J. Hone, Q. Lin, *Nanoscale* **2016**, *8*, 5815.
[23] Z. Pu, J. Tu, R. Han, X. Zhang, J. Wu, C. Fang, H. Wu, X. Zhang, H. Yu, D. Li, *Lab Chip* **2018**, *18*, 3570.
[24] W. Fu, L. Feng, G. Panaitov, D. Kireev, D. Mayer, A. Offenhäusser, H.-J. Krause, *Sci. Adv.* **2017**, *3*, e1701247.
[25] C. Wang, J. Kim, Y. Zhu, J. Yang, G. H. Lee, S. Lee, J. Yu, R. Pei, G. Liu, C. Nuckolls, J. Hone, Q. Lin, *Biosens. Bioelectron.* **2015**, *71*, 222.
[26] J. H. An, S. J. Park, O. S. Kwon, J. Bae, J. Jang, *ACS Nano* **2013**, *7*, 10563.
[27] Y. Zhu, Y. Li, G. Arefe, R. A. Burke, C. Tan, Y. Hao, X. Liu, X. Liu, W. J. Yoo, M. Dubey, Q. Lin, J. C. Hone, *Nano Lett.* **2018**, *18*, 3807.
[28] Y. Ohno, K. Maehashi, K. Matsumoto, *J. Am. Chem. Soc.* **2010**, *132*, 18012.
[29] C. Wang, W. Ye, Y. Li, Y. Zhu, Q. Lin, M. He, *Biosens. Bioelectron.* **2019**, *129*, 93.
[30] S. Farid, X. Meshik, M. Choi, S. Mukherjee, Y. Lan, D. Parikh, S. Poduri, U. Baterdene, C. E. Huang, Y. Y. Wang, P. Burke, M. Dutta, M. A. Stroscio, *Biosens. Bioelectron.* **2015**, *71*, 294.
[31] M. Ku, J. Kim, J. E. Won, W. Kang, Y. G. Park, J. Park, J. H. Lee, J. Cheon, H. H. Lee, J. U. Park, *Sci. Adv.* **2020**, *6*, eabb2891.
[32] O. S. Kwon, S. J. Park, J. Y. Hong, A. R. Han, J. S. Lee, J. S. Lee, J. H. Oh, J. Jang, *ACS Nano* **2012**, *6*, 1486.
[33] J. Sabaté del Río, O. Y. F. Henry, P. Jolly, D. E. Ingber, *Nat. Nanotechnol.* **2019**, *14*, 1143.
[34] M. Bariya, H. Y. Y. Nyein, A. Javey, *Nat. Electron.* **2018**, *1*, 160.
[35] Y. Yang, Y. Song, X. Bo, J. Min, O. S. Pak, L. Zhu, M. Wang, J. Tu, A. Kogan, H. Zhang, T. K. Hsiai, Z. Li, W. Gao, *Nat. Biotechnol.* **2020**, *38*, 217.
[36] W. Gao, S. Emaminejad, H. Y. Y. Nyein, S. Challa, K. Chen, A. Peck, H. M. Fahad, H. Ota, H. Shiraki, D. Kiriya, D. H. Lien, G. A. Brooks, R. W. Davis, A. Javey, *Nature* **2016**, *529*, 509.
[37] Y. Song, J. Min, Y. Yu, H. Wang, Y. Yang, H. Zhang, W. Gao, *Sci. Adv.* **2020**, *6*, eaay9842.
[38] Y. Yang, X. Yang, X. Zou, S. Wu, D. Wan, A. Cao, L. Liao, Q. Yuan, X. Duan, *Adv. Funct. Mater.* **2017**, *27*, 1604096.
[39] H. Jang, Y. J. Park, X. Chen, T. Das, M. S. Kim, J. H. Ahn, *Adv. Mater.* **2016**, *28*, 4184.
[40] Z. Hao, Z. Wang, Y. Li, Y. Zhu, X. Wang, C. G. De Moraes, Y. Pan, X. Zhao, Q. Lin, *Nanoscale* **2018**, *10*, 21681.
[41] Z. Hao, Y. Pan, C. Huang, Z. Wang, Q. Lin, X. Zhao, S. Liu, *ACS Sens.* **2020**, *5*, 2503.
[42] Z. Hao, Y. Pan, W. Shao, Q. Lin, X. Zhao, *Biosens. Bioelectron.* **2019**, *134*, 16.
[43] L. Antoury, N. Hu, L. Balaj, S. Das, S. Georghiou, B. Darras, T. Clark, X. O. Breakefield, T. M. Wheeler, *Nat. Commun.* **2018**, *9*, 3906.
[44] R. Sha, N. Vishnu, S. Badhulika, *Sens. Actuators, B* **2019**, *279*, 53.